

Supporting Information
for
Diversifying NMR Supersequences with New
HSQC-based Modules

Jonathan R. J. Yong,¹ Alexandar L. Hansen,² Ēriks Kupče,³ Tim D. W.
Claridge^{1,*}

¹ *Chemistry Research Laboratory, Department of Chemistry, University of Oxford,
Mansfield Road, Oxford, OX1 3TA, U.K.*

² *Campus Chemical Instrument Center, The Ohio State University, 460 W. 12th Avenue,
Columbus, OH, 43210 U.S.*

³ *Bruker UK Ltd., Banner Lane, Coventry, CV4 9GH, U.K.*

* tim.claridge@chem.ox.ac.uk

Contents

1 Product operator analysis for pulse sequences	S3
2 Origin and suppression of wing artefacts	S4
3 Effect of setting $\Delta' = 1/(4 \cdot {}^1J_{\text{CH}})$ in seHSQC	S8
4 Comparison of BIG-BIRD and ZIP elements	S9
5 Multiplicity editing in seHSQC	S10
6 Summary of ${}^{13}\text{C}$ seHSQC sensitivity comparisons	S11
7 Retention of bulk magnetisation by ${}^{15}\text{N}$ modules	S13
8 ${}^{15}\text{N}$ HSQC and line broadening	S14
9 Effect of lengthened gradients in ${}^{15}\text{N}$ modules	S15
10 Effect of k-scaling	S16
11 HSQC-TOCSY/HSQC sensitivity comparisons	S21
12 Other example spectra	S25

1 Product operator analysis for pulse sequences

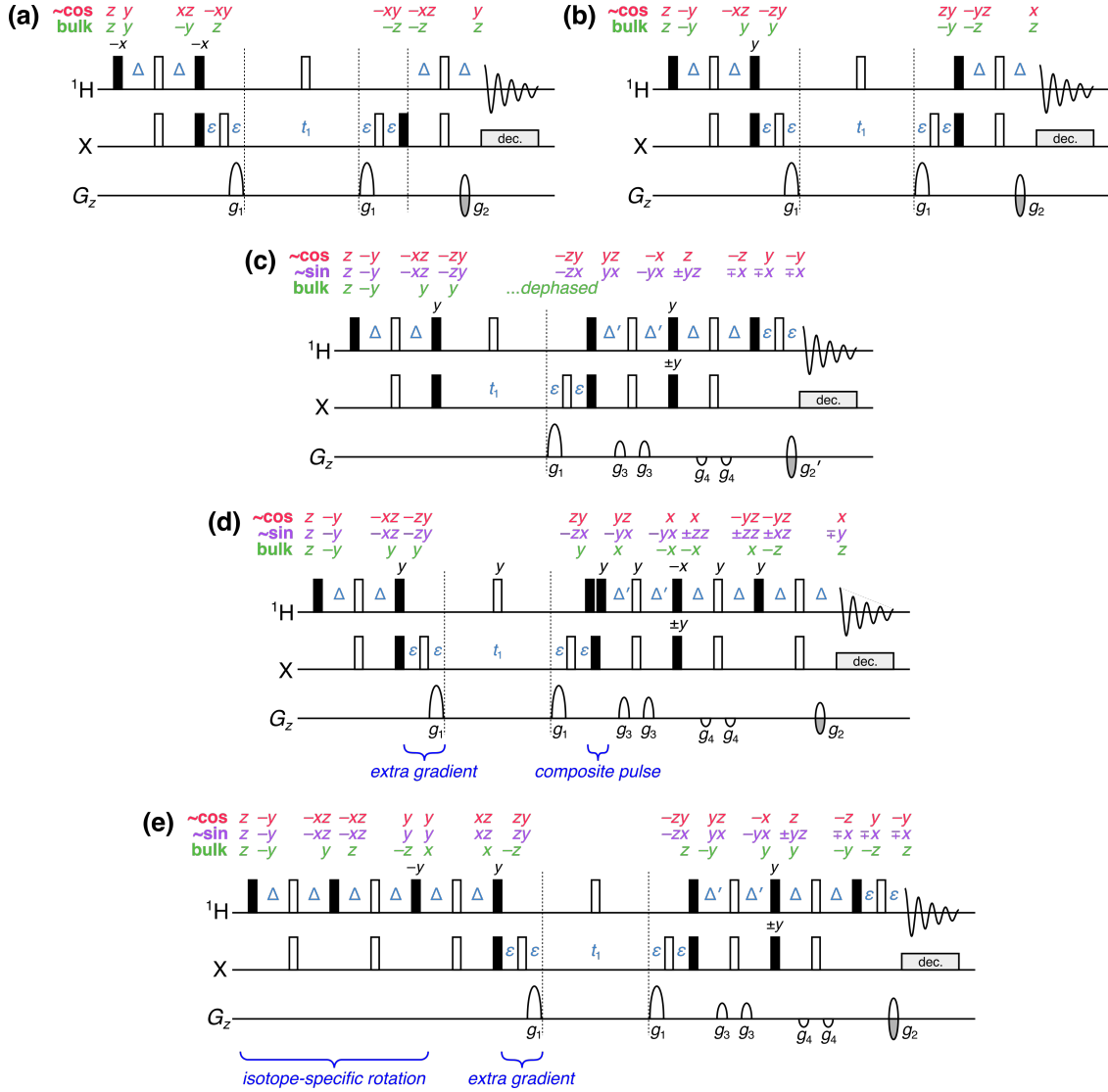


Figure S1: Product operators for an IS spin system at each stage of the HSQC and seHSQC sequences described in the main text. One-letter terms m ($m \in \{x, y, z\}$) are shorthand for single-spin terms on proton, i.e. \hat{I}_m . Two-letter terms mn are shorthand for two-spin terms on both the proton and heteronucleus, i.e. $2\hat{I}_m\hat{S}_n$. “ $\sim\cos$ ” represents the pathway for ${}^1\text{H}^{\text{C}}$ magnetisation that is cosine-modulated after t_1 : for the HMQC and HSQC, this is the only component that is detected. For the seHSQC, the sine-modulated ${}^1\text{H}^{\text{C}}$ component (labelled with “ $\sim\sin$ ”) is also detected. “bulk” refers to the bulk ${}^1\text{H}^{\text{C}}$ magnetisation, i.e. protons that are not directly coupled to the heteronucleus. Note that this analysis assumes $\Delta = \Delta' = 1/(4 \cdot {}^1J_{\text{XH}})$. All other symbols have the same meaning as in Figure 1 of the main text. (a) NOAH HMQC (“M”). (b) NOAH HSQC (“S”). (c) Cavanagh–Rance–Kay seHSQC; notice that the bulk magnetisation is dephased by the lone t_1 gradient. (d) NOAH seHSQC, version 1 (“ S_1^+ ”). (e) NOAH seHSQC, version 2 (“ S_2^+ ”). Immediately following the ZIP pulse sequence element, directly bonded protons are rotated onto $+y$, whereas the bulk magnetisation is rotated onto $+x$.

2 Origin and suppression of wing artefacts

The origin of the “wing” artefacts in the final homonuclear modules can be most clearly seen from the following series of experiments involving the NOAH-3 ^{15}N seHSQC/ ^{13}C ZIP-seHSQC/CLIP-COSY ($\text{S}_\text{N}^+\text{S}_2^+\text{C}^\text{c}$) supersequence. As described in the main text, if the extra gradient before t_1 is not present, each peak in the COSY with an indirect-dimension frequency of $f_1 = \Omega_\text{H}$ is flanked by a pair of artefacts at

$$f_1 = \Omega_\text{H} \pm \Omega_\text{H} \cdot \left(\frac{\text{SW}_{\text{COSY}}}{2 \cdot \text{SW}_{\text{HSQC}}} \right),$$

where Ω_H is the offset of the relevant proton and SW refers to the indirect-dimension spectral width. Since the f_1 spectral widths of the two seHSQC modules are different, they lead to distinct sets of wing artefacts in the COSY. In the spectra shown in the following figures, we have

$$\text{SW}_{^{15}\text{N HSQC}} = 2128 \text{ Hz}$$

$$\text{SW}_{^{13}\text{C HSQC}} = 23810 \text{ Hz}$$

$$\text{SW}_{\text{COSY}} = 8418 \text{ Hz}$$

meaning that the artefacts coming from the ^{15}N seHSQC occur at $f_1 = (1.00 \pm 1.98)\Omega_\text{H}$ (and are therefore often folded), whereas artefacts coming from the ^{13}C seHSQC occur at $f_1 = (1.00 \pm 0.18)\Omega_\text{H}$ (and are typically found very close to the main peak). In both cases, the artefacts associated with intense methyl group peaks are the most obvious, but similar artefacts are observed for all other peaks, albeit with lower absolute intensities.

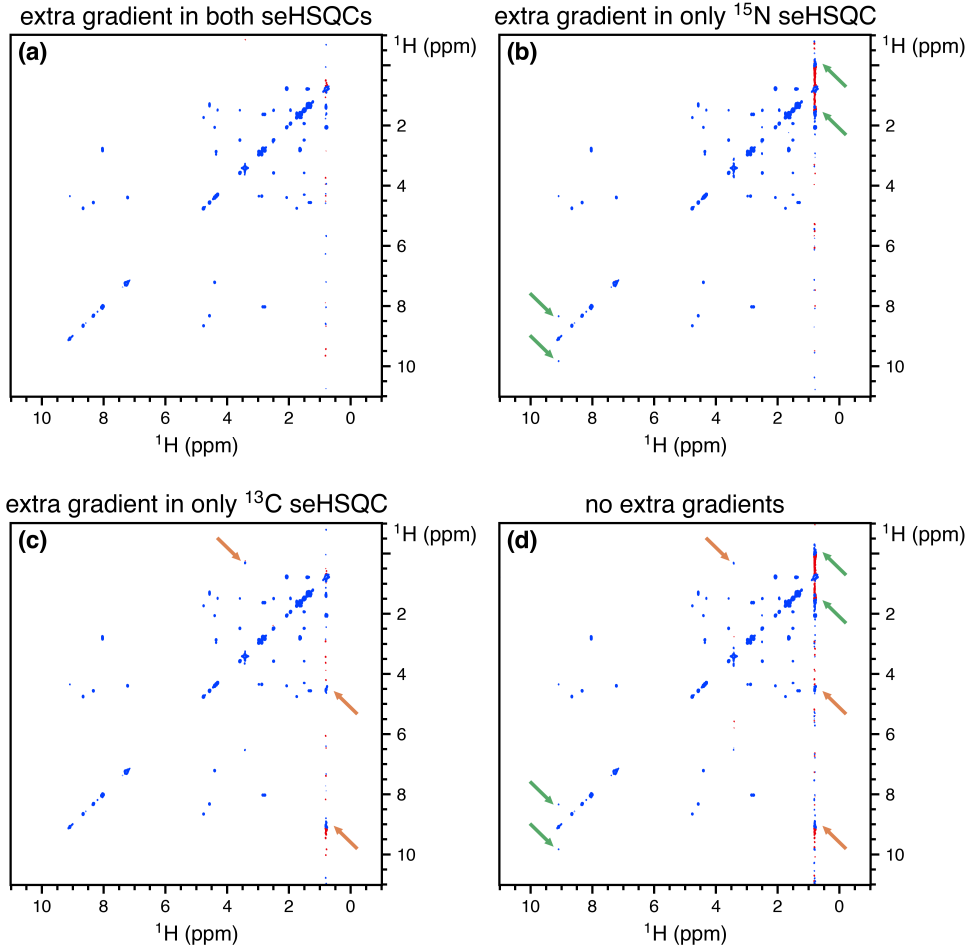


Figure S2: CLIP-COSY spectra obtained from various forms of the NOAH-3 $S_N^+S_2^+C^c$ supersequence. Wing artefacts arising from the ^{15}N seHSQC are highlighted in orange; those arising from the ^{13}C seHSQC in green. Notice how (in this case) the former can easily be misinterpreted as a crosspeak, while the latter obscures genuine crosspeaks. **(a)** With the extra gradient inserted for both modules, i.e. no artefacts. **(b)** With an extra gradient in only the ^{15}N module, i.e. only the ^{13}C artefacts. **(c)** With an extra gradient in only the ^{13}C module. **(d)** With no extra gradients. Spectra were obtained on a 700 MHz Bruker AV III equipped with a TCI H/C/N cryoprobe; the sample used was 40 mM gramicidin in DMSO- d_6 .

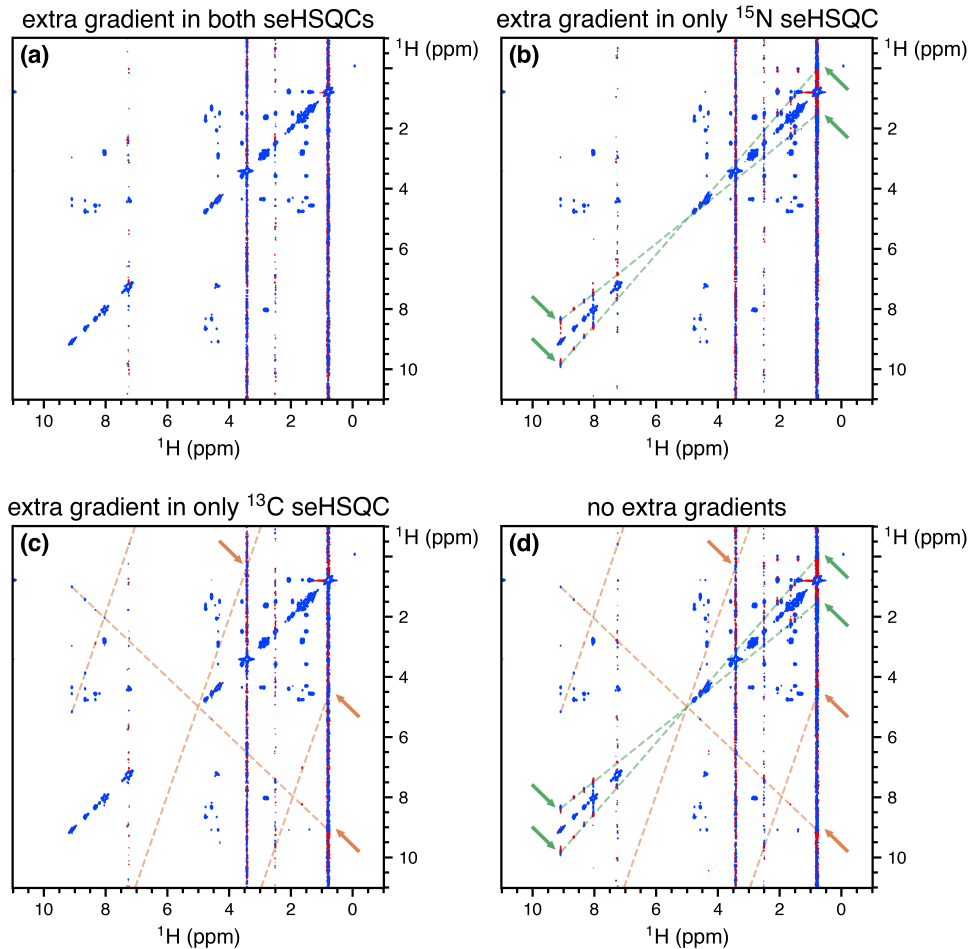


Figure S3: The same spectra as Figure S2, but plotted with a smaller base contour level to illustrate the regular indirect-dimension frequencies of the wing artefacts. A greater number of artefacts are now visible (in addition to those already highlighted in Figure S2, which are still marked with arrows). The artefacts arising from the ^{15}N seHSQC lie on the orange dotted line; those arising from the ^{13}C seHSQC lie on the green dotted line. **(a)** With the extra gradient inserted for both modules, i.e. no artefacts. **(b)** With an extra gradient in only the ^{15}N module, i.e. only the ^{13}C artefacts. **(c)** With an extra gradient in only the ^{13}C module. **(d)** With no extra gradients. Spectra were obtained on a 700 MHz Bruker AV III equipped with a TCI H/C/N cryoprobe; the sample used was 40 mM gramicidin in DMSO- d_6 .

Additional information can be gleaned from the following series of CLIP-COSY spectra, obtained from NOAH-2 $S_2^+ C^c$ supersequences. In the seHSQC module, the two gradients g_1 in the t_1 period are independently enabled or disabled (by setting their amplitude to 0). Traces of the resulting CLIP-COSY spectra are shown in Figure S4. The gradients serve to dephase any bulk $^1\text{H}^{13}\text{C}$ magnetisation that is transverse during either half of t_1 : therefore, if (for example) the gradient in the first half of t_1 is switched off, this allows bulk magnetisation that is transverse in the first half of t_1 to evolve and ultimately contribute to the wing artefacts in the CLIP-COSY. As can be seen, gradients must be applied in *both* halves for complete suppression of the wing artefacts.

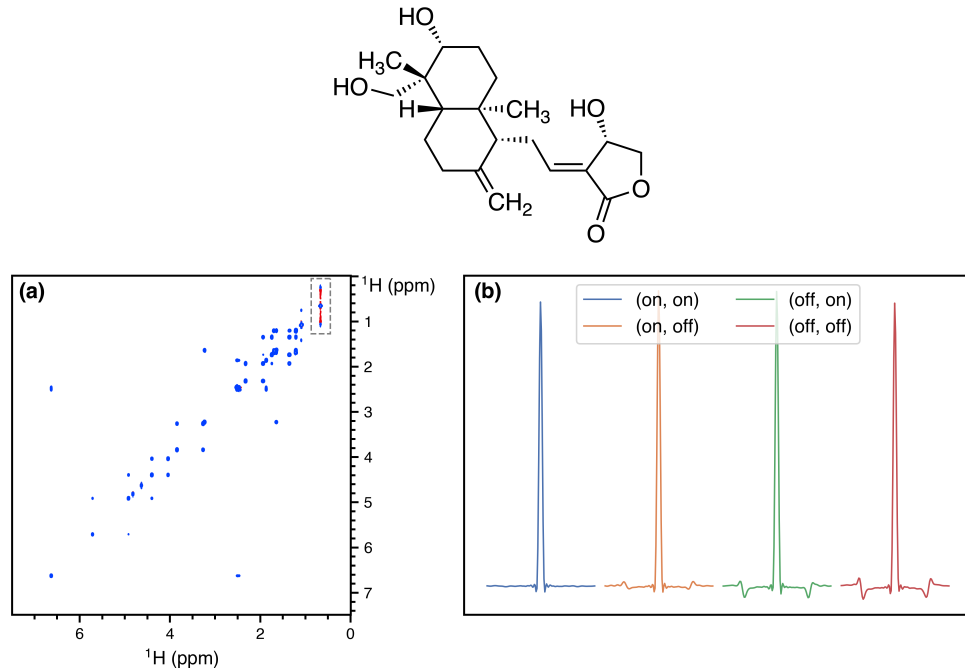


Figure S4: (a) CLIP-COSY spectrum obtained from NOAH-2 $S_2^+ C^c$ sequence, where both gradients in t_1 were disabled (i.e. “(off, off)”). The other three CLIP-COSY spectra are similar, except that the (on, on) spectrum (with gradients applied in both halves of t_1) does not have wing artefacts (grey box). (b) f_1 traces through 0.67 ppm of the four CLIP-COSY spectra obtained with various combinations of gradients, corresponding to the boxed area in (a). Only the (on, on) spectrum (in blue) is free from wing artefacts. The (on, off) and (off, on) spectra (in orange and green respectively) have wing artefacts arising from bulk magnetisation that evolves during the second and first halves of the seHSQC t_1 period respectively. The (off, off) spectrum (red), which corresponds to the 2D spectrum in (a), has the greatest intensity of wing artefacts. Spectra were obtained on a 700 MHz Bruker AV III equipped with a TCI H/C/N cryoprobe; the sample used was 40 mM andrographolide in $\text{DMSO}-d_6$.

3 Effect of setting $\Delta' = 1/(4 \cdot {}^1J_{CH})$ in seHSQC

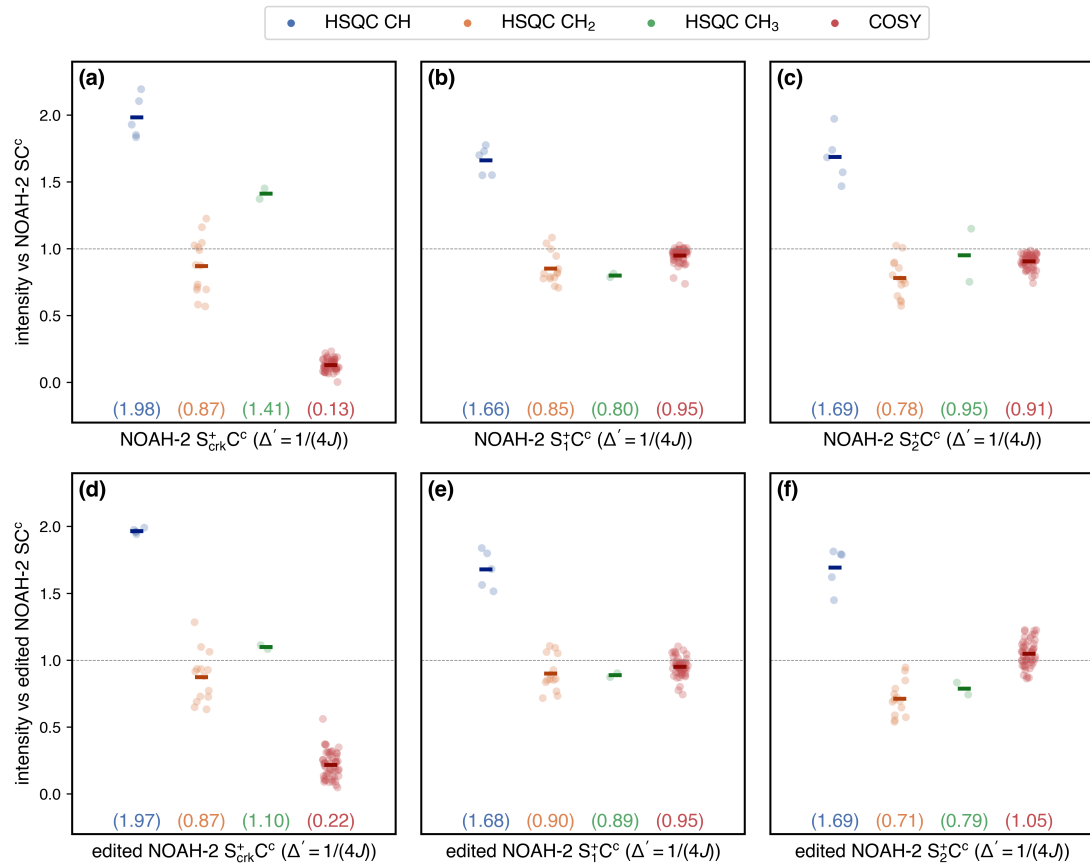


Figure S5: Sensitivity of NOAH-2 S⁺C^c supersequences with Δ' set to $1/(4 \cdot {}^1J_{CH})$, versus the corresponding NOAH-2 SC^c supersequence (i.e. unedited for (a)–(c), edited for (d)–(f)). (a) CRK seHSQC, without multiplicity editing. (b) S₁⁺ module, without multiplicity editing. (c) S₂⁺ module, without multiplicity editing. (d) CRK seHSQC, with multiplicity editing. (e) S₁⁺ module, with multiplicity editing. (f) S₂⁺ module, with multiplicity editing. Spectra were obtained on a 700 MHz Bruker AV III equipped with a TCI H/C/N cryoprobe; the sample used was 40 mM andrographolide in DMSO-*d*₆.

By setting $\Delta' = 1/(4 \cdot {}^1J_{CH})$, theory predicts a larger sensitivity enhancement for CH peaks, whereas CH₂ and CH₃ peaks should have the same sensitivity as in the unenhanced HSQC. This is true for both the S₁⁺ and S₂⁺ modules, as can be seen by comparing Figures 2b and 2c (which show $\Delta' = 1/(8 \cdot {}^1J_{CH})$) to Figures S5b and S5c (which show $\Delta' = 1/(4 \cdot {}^1J_{CH})$). At the same time, for CH₂ and CH₃ peaks, we observe sensitivity losses even relative to the unenhanced HSQC; this is likely due to pulse imperfections in the longer pulse sequence and is in line with previous studies (ref. 13 of the main text).

4 Comparison of BIG-BIRD and ZIP elements

The BIG-BIRD element used here was $45^\circ_{45^\circ}(^1\text{H}) - 2\Delta - 180^\circ(^1\text{H}, ^{13}\text{C}) - 2\Delta - 45^\circ_{225^\circ}(^1\text{H})$ for the unedited NOAH seHSQC, where β_ϕ indicates a hard pulse with flip angle β and phase ϕ , and $\Delta = 1/(4 \cdot ^1J_{\text{CH}})$. For the edited NOAH seHSQC, the BIG-BIRD pulse phases are slightly modified to give $45^\circ_{315^\circ}(^1\text{H}) - 2\Delta - 180^\circ(^1\text{H}, ^{13}\text{C}) - 2\Delta - 45^\circ_{135^\circ}(^1\text{H})$. These, and the ZIP, have the same net effect on $^1\text{H}^{\text{C}}$ and $^1\text{H}^{!C}$ magnetisation, as can be seen from the product operator analysis in Figure S1. Thus, they can be used interchangeably in version 2 of the NOAH seHSQC. However, the ZIP provides greater sensitivity in both the HSQC and downstream COSY (Figure S6).

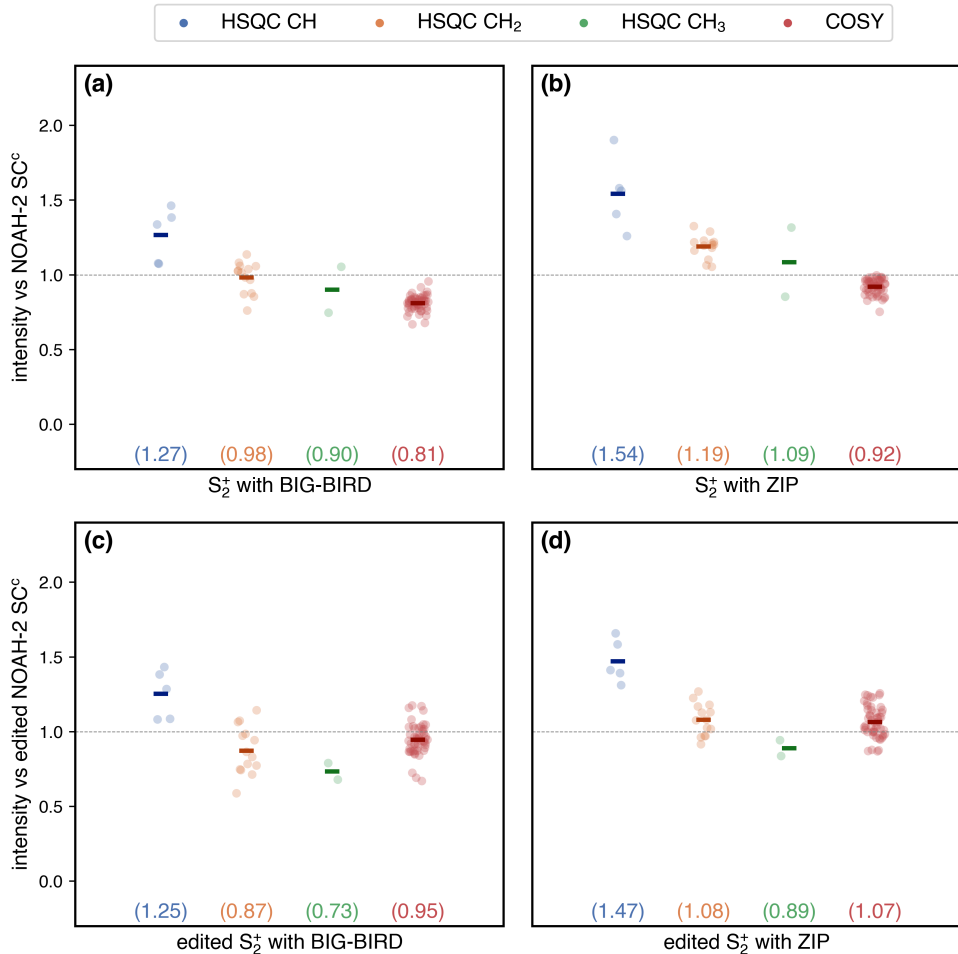


Figure S6: Sensitivity of NOAH-2 $S_2^+ \text{C}^{\text{c}}$ supersequences with either BIG-BIRD or ZIP elements, versus the corresponding NOAH-2 SC^{c} supersequences (i.e. unedited for (a) and (b), edited for (c) and (d)). The value of Δ' was set to $1/(8 \cdot ^1J_{\text{CH}})$. (a) Using the unedited NOAH seHSQC with the BIG-BIRD element. (b) Unedited seHSQC with ZIP. (c) Edited seHSQC with BIG-BIRD. (d) Edited seHSQC with ZIP. Spectra were obtained on a 700 MHz Bruker AV III equipped with a TCI H/C/N cryoprobe; the sample used was 40 mM andrographolide in DMSO-*d*₆.

5 Multiplicity editing in seHSQC

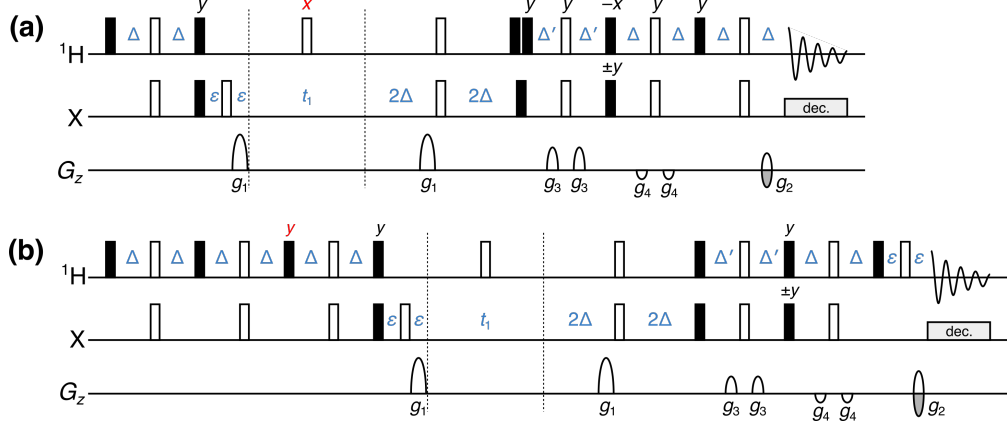


Figure S7: Implementation of multiplicity editing in the new NOAH seHSQC modules. Pulse phases which differ from the unedited versions (Figure S1) are highlighted in red; these are needed to compensate for the extra ¹H 180° pulse in the editing period. Symbols have the same meaning as in Figure 1 of the main text. (a) NOAH seHSQC, version 1 ("S₁⁺"). (b) NOAH seHSQC, version 2 ("S₂⁺").

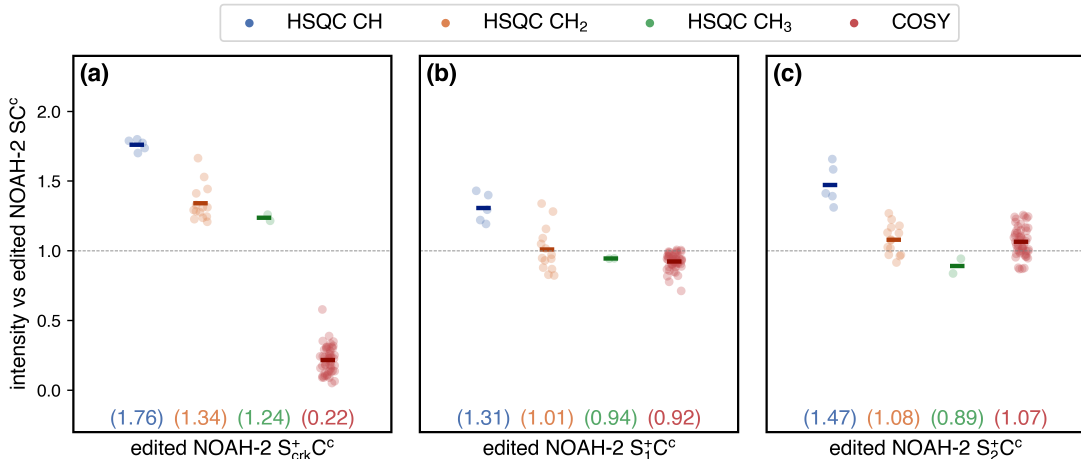


Figure S8: Sensitivity of multiplicity-edited S⁺C^c supersequences, relative to the SC^c supersequence. Spectra were obtained with $\Delta' = 1/(8 \cdot ^1J_{CH})$. (a) Using the CRK seHSQC. (b) Using the S₁⁺ module. (c) Using the S₂⁺ module. Spectra were obtained on a 700 MHz Bruker AV III equipped with a TCI H/C/N cryoprobe; the sample used was 40 mM andrographolide in DMSO-d₆.

On average, both versions of the NOAH seHSQC provide sensitivity gains for HSQC CH and CH₂ peaks (Figures S8b and S8c) while not compromising the COSY intensities as the CRK seHSQC does (Figure S8a). The S₂⁺ module in particular provides slightly better performance. Note also how the COSY intensities with the S₂⁺ module are on average higher than with the original HSQC module: this indicates that the S₂⁺ module preserves bulk ¹H!¹³C magnetisation better. As discussed in the main text, this is because the bulk magnetisation is longitudinal during the editing period.

6 Summary of ^{13}C seHSQC sensitivity comparisons

Experiment		HSQC			COSY	Figure	
edited?	HSQC variant	Δ'	CH	CH_2	CH_3		
no	HSQC	–	1.00*	1.00*	1.00*	1.00*	–
	CRK seHSQC	1/(8J)	1.80	1.32	1.58	0.13	2a
	NOAH seHSQC v1	1/(8J)	1.29	0.94	0.89	0.94	2b
	NOAH seHSQC v2	1/(8J)	1.54	1.19	1.09	0.92	2c
	CRK seHSQC	1/(4J)	1.98	0.87	1.41	0.13	S5a
	NOAH seHSQC v1	1/(4J)	1.66	0.85	0.80	0.95	S5b
	NOAH seHSQC v2	1/(4J)	1.69	0.78	0.95	0.91	S5c
	no HSQC, only COSY	–	–	–	–	1.09	–
yes	HSQC	–	1.00†	1.00†	1.00†	1.00†	–
	CRK seHSQC	1/(8J)	1.76	1.34	1.24	0.22	S8a
	NOAH seHSQC v1	1/(8J)	1.31	1.01	0.94	0.92	S8b
	NOAH seHSQC v2	1/(8J)	1.47	1.08	0.89	1.07	S8c
	CRK seHSQC	1/(4J)	1.97	0.87	1.10	0.22	S5d
	NOAH seHSQC v1	1/(4J)	1.68	0.90	0.89	0.95	S5e
	NOAH seHSQC v2	1/(4J)	1.69	0.71	0.79	1.05	S5f
	no HSQC, only COSY	–	–	–	–	1.29	–

Table S1: Relative sensitivities of HSQC and CLIP-COSY spectra in NOAH-2 SC^c and S⁺C^c supersequences. All sensitivities are normalised against the corresponding SC^c sequences: in particular, the unedited seHSQC supersequences are compared against the unedited SC^c (marked with *), and likewise edited seHSQC supersequences are compared against the edited SC^c (marked with †). Note that the two standalone CLIP-COSY entries (the last row in both sections) refer to the same spectrum, and therefore have the same *absolute* sensitivity. The difference in the *relative* sensitivity arises only because they are being compared against the COSY intensities in different reference supersequences, which is done here for consistency with the other figures in this text. See Table S2 for a version of this table where the COSY sensitivities in both unedited and edited supersequences are normalised against the standalone CLIP-COSY. Spectra were obtained on a 700 MHz Bruker AV III equipped with a TCI H/C/N cryoprobe; the sample used was 40 mM andrographolide in DMSO-*d*₆.

edited?	HSQC variant	Δ'	HSQC			COSY
			CH	CH ₂	CH ₃	
no	HSQC	–	1.00*	1.00*	1.00*	0.93
	CRK seHSQC	1/(8J)	1.80	1.32	1.58	0.12
	NOAH seHSQC v1	1/(8J)	1.29	0.94	0.89	0.88
	NOAH seHSQC v2	1/(8J)	1.54	1.19	1.09	0.85
	CRK seHSQC	1/(4J)	1.98	0.87	1.41	0.12
	NOAH seHSQC v1	1/(4J)	1.66	0.85	0.80	0.88
	NOAH seHSQC v2	1/(4J)	1.69	0.78	0.95	0.84
	no HSQC, only COSY	–	–	–	–	1.00‡
yes	HSQC	–	1.00†	1.00†	1.00†	0.79
	CRK seHSQC	1/(8J)	1.76	1.34	1.24	0.17
	NOAH seHSQC v1	1/(8J)	1.31	1.01	0.94	0.73
	NOAH seHSQC v2	1/(8J)	1.47	1.08	0.89	0.84
	CRK seHSQC	1/(4J)	1.97	0.87	1.10	0.17
	NOAH seHSQC v1	1/(4J)	1.68	0.90	0.89	0.75
	NOAH seHSQC v2	1/(4J)	1.69	0.71	0.79	0.82
	no HSQC, only COSY	–	–	–	–	1.00‡

Table S2: Relative sensitivities of HSQC and CLIP-COSY spectra in NOAH-2 SC^c and S⁺C^c supersequences. All HSQC sensitivities are normalised against the HSQC spectrum in the corresponding SC^c sequences: in particular, the unedited seHSQCs are compared against the unedited HSQC (marked with *), and likewise edited seHSQCs are compared against the edited HSQC (marked with †). All COSY sensitivities are compared against the standalone CLIP-COSY spectrum (the last row in both sections, marked with ‡). This is different from the figures used in this text, which compare the COSY intensities against the COSY component of the corresponding SC^c supersequence. See Table S1 for a version of this table which is consistent with the other figures in this text. Spectra were obtained on a 700 MHz Bruker AV III equipped with a TCI H/C/N cryoprobe; the sample used was 40 mM andrographolide in DMSO-*d*₆.

7 Retention of bulk magnetisation by ^{15}N modules

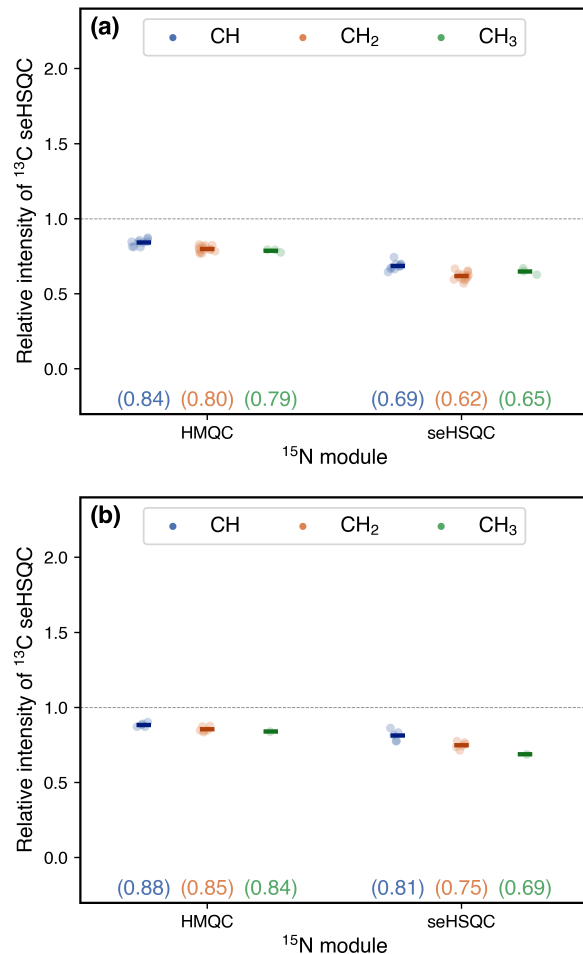


Figure S9: Signal intensities of the ^{13}C seHSQC in NOAH-3 $\text{XS}_2^+ \text{C}^{\text{c}}$ supersequences, normalised against a reference ^{13}C seHSQC taken from a NOAH-2 $\text{S}_2^+ \text{C}^{\text{c}}$ supersequence. The module X is either the ^{15}N HMQC (M) or the ^{15}N seHSQC (S_N^+); the numbers indicate the amount of $^1\text{H}^{\text{C}}$ magnetisation that is preserved by the ^{15}N module. (a) Using 40 mM gramicidin in DMSO- d_6 . (b) Using 50 mM zolmitriptan in DMSO- d_6 . Spectra were obtained on a 700 MHz Bruker AV III equipped with a TCI H/C/N cryoprobe.

8 ^{15}N HSQC and line broadening

For $^{15}\text{N}-^1\text{H}$ correlations, both the HMQC and version 2 of the new seHSQC are recommended as they keep the bulk magnetisation (both $^1\text{H}^{\text{C}}$ and $^1\text{H}^{\text{IX}}$) along $\pm z$ during the t_1 period. The HSQC module, as well as version 1 of the seHSQC, place this magnetisation in the xy -plane during t_1 , leading to J_{HH} evolution; consequently, the amount of bulk magnetisation “passed on” to the downstream modules decreases as the ^{15}N t_1 is increased. Since t_1 for each NOAH module is incremented in sync, this is manifested in downstream modules as a t_1 -dependent decrease in amplitude, or f_1 line broadening after Fourier transformation, as shown in Figure S10.

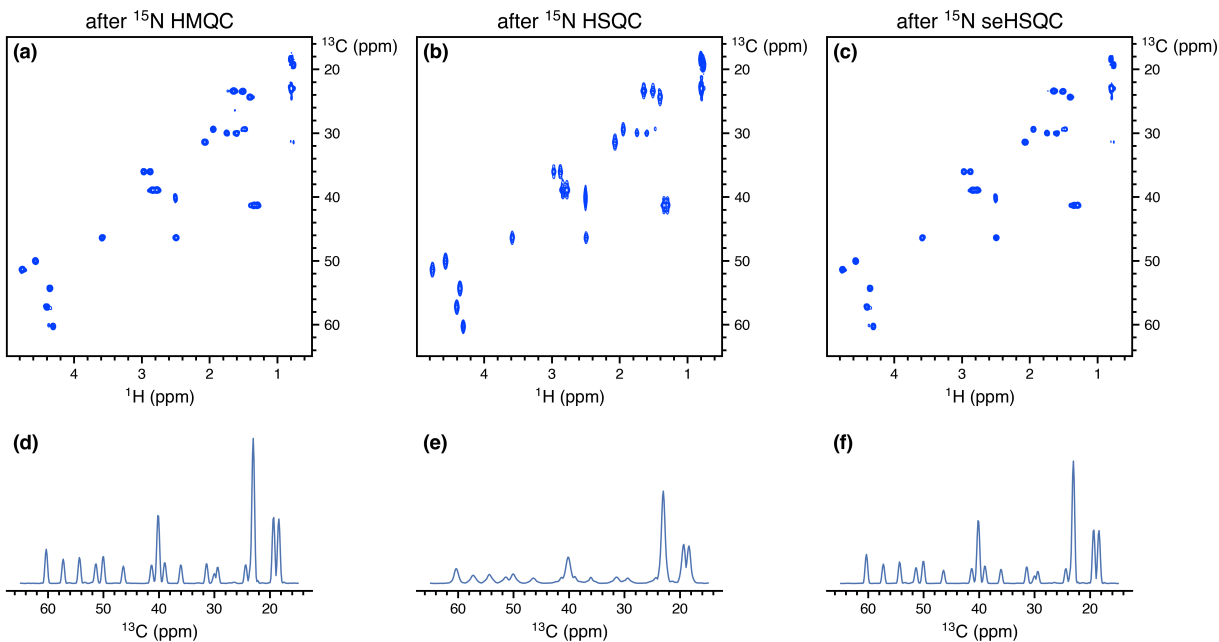


Figure S10: ^{13}C seHSQC spectra obtained from NOAH-3 $\text{XS}_2^+ \text{Cc}$ (^{15}N module + ^{13}C seHSQC + CLIP-COSY) supersequences. The ^{15}N spectral window was 30 ppm and 256 t_1 increments were collected, corresponding to an indirect-dimension ^{15}N acquisition time of 60.1 ms. (a) X = HMQC (“M”). (b) X = HSQC (“S”). (c) X = seHSQC (“ S_N^+ ”). (d)–(f) Projections of spectra (a)–(c) onto the f_1 axis. Note the f_1 line broadening in (b) and (e). Spectra were obtained on a 700 MHz Bruker AV III equipped with a TCI H/C/N cryoprobe; the sample used was 40 mM gramicidin in $\text{DMSO}-d_6$.

This line broadening also leads to a substantial sensitivity loss (for example, across all peaks, the ^{13}C seHSQC in Figure S10b has almost 65% lower sensitivity than that in Figure S10a). The extent of the line broadening depends on the acquisition time, and is particularly pronounced for long acquisition times, i.e. small ^{15}N spectral windows. In our experience, at ^{15}N acquisition times of ca. 5 ms the effect is almost indiscernible. Such a short acquisition time would lead to poor resolution in the ^{15}N dimension itself, which may or may not be tolerable. Of course, this issue can be entirely avoided by using either the HMQC or seHSQC.

9 Effect of lengthened gradients in ^{15}N modules

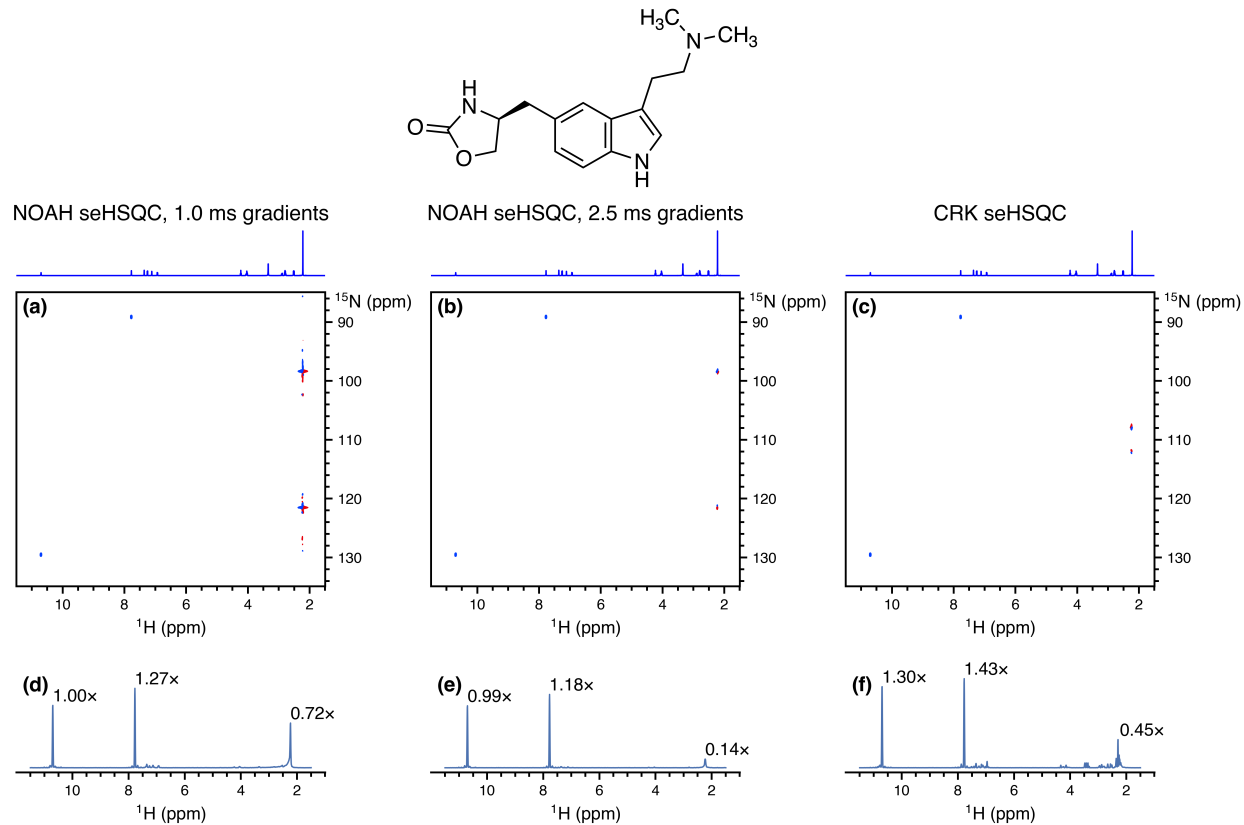


Figure S11: ^{15}N seHSQC spectra obtained using the NOAH and CRK implementations. The peaks at 7.8 and 10.7 ppm (^1H shifts) are genuine crosspeaks; the mixed-phase peaks at 2.2 ppm are artefacts. The 1D ^1H spectrum is shown above each of the 2D spectra in (a)–(c); the artefacts seen in the 2D correspond to the intense N -methyl groups at 2.2 ppm. (a) NOAH seHSQC, with original CTP gradients of 1 ms. (b) NOAH seHSQC, with longer CTP gradients of 1 ms. (c) Standalone CRK seHSQC with 1 ms CTP gradients (Bruker `hsqcetf3gpsi2` pulse programme). (d)–(f) Projections of spectra (a)–(c) onto the f_2 axis. The numbers indicate relative peak heights (normalised against the 10.7 ppm peak in (d)). Spectra were obtained on a 700 MHz Bruker AV III equipped with a TCI H/C/N cryoprobe; the sample used was 50 mM zolmitriptan in $\text{DMSO}-d_6$.

The lengthening of CTP gradients from 1 ms to 2.5 ms is aimed at cleaning up artefacts arising from bulk magnetisation that is not properly returned to $+z$ at the end of the sequence. Figure S11 shows exactly how effective this strategy is. In (d), where the CTP gradients have their original duration, the artefacts originating from the intense methyl groups have comparable intensity to the desired peaks. When the gradients are lengthened in (e), the crosspeak intensities are almost unaffected, whereas the artefacts are suppressed by a factor of 5 or more. Although this suppression is not complete, this should not be interpreted as a weakness of the new NOAH seHSQC module, as similar artefacts are also visible in the CRK seHSQC (f). Indeed, every $^{15}\text{N}-^1\text{H}$ experiment we tested has at least *some* artefact intensity in this region.

10 Effect of k -scaling

The effect of k -scaling on the HMQC is shown in Figure S12. By decreasing the indirect dimension resolution, the f_1 linewidths of the peaks increase: this can lead to significant sensitivity enhancement for the HMQC (up to $2.7\times$), because J_{HH} splitting in the f_1 dimension is no longer resolved. The largest gains are observed for peaks where J_{HH} splitting is more visible; for the leftmost peak at $\delta_N = 128$ ppm which has no resolved J_{HH} splitting, only a more modest $1.7\times$ gain in sensitivity is attained.

For the seHSQC module, k -scaling on its own leads to far smaller sensitivity gains (Figure S13). Any increase in the total peak volume is almost completely offset by the f_1 broadening. Therefore, even at $k = 8$, the largest sensitivity gains that can be attained are $\sim 1.3\times$.

The use of linear prediction for spectra with $k > 1$ can, to a certain extent, compensate for the line broadening. This is less successful for the HMQC spectra (Figure S14). Although raw gains in peak height can be observed for all values of k , there is a corresponding decrease in the spectral quality, as evidenced by the f_1 multiplet structure being increasingly distorted. On the other hand, linear prediction performs well for the seHSQC spectra (Figure S15), where there is no multiplet structure in f_1 . Even the reconstruction with $k = 8$ has reasonable spectral quality: although the 2D spectrum (d) appears to have unusual peak shapes, this is merely the result of having the same contour levels as the $k = 1$ spectrum. The actual peaks are still clearly singlets, as can be seen from the projection in (h).

An additional example of successful k -scaling and linear prediction (with $k = 4$) can be seen in Section 12.

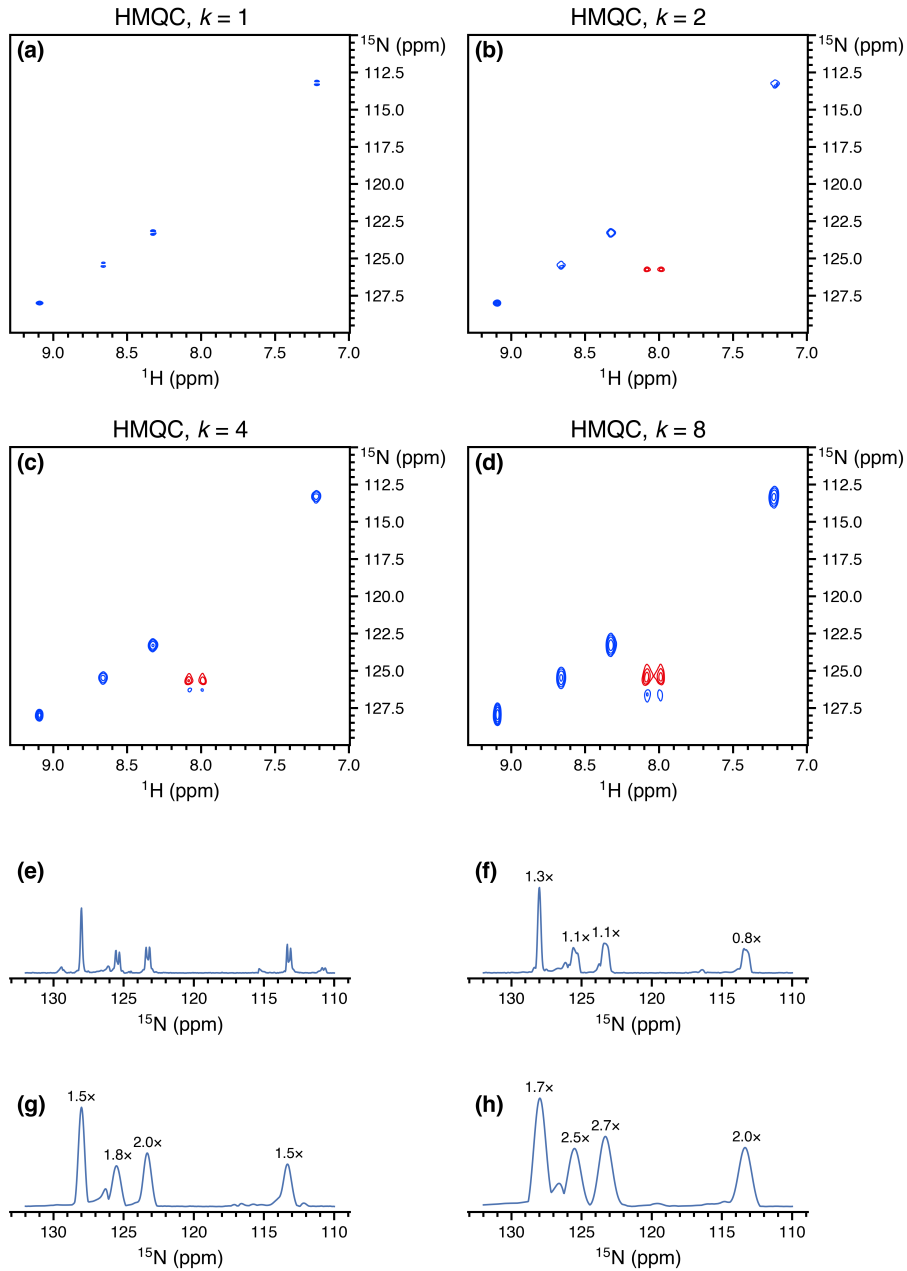


Figure S12: (HMQC without linear prediction.) ¹⁵N HMQC spectra (from NOAH-3 MS₂⁺C^c supersequences) obtained with various values of the scaling factor k . The peak at $\delta_{\text{H}} = 8.03$ ppm is a folded peak from the ornithine $\delta\text{-NH}_2$. (a) $k = 1$, with 256 t_1 increments and 2 scans per increment (denoted as 256 : 2). (b) $k = 2$, i.e. effectively 128 t_1 increments and 4 scans per increment (128 : 4). (c) $k = 4$ (64 : 8). (d) $k = 8$ (32 : 16). (e)–(h) Projections of 2D spectra in (a)–(d) onto the f_1 axis, shown at the same noise level. Numbers indicate peak heights relative to the $k = 1$ HMQC spectrum. Spectra were obtained on a 700 MHz Bruker AV III equipped with a TCI H/C/N cryoprobe; the sample used was 40 mM gramicidin in DMSO-*d*₆.

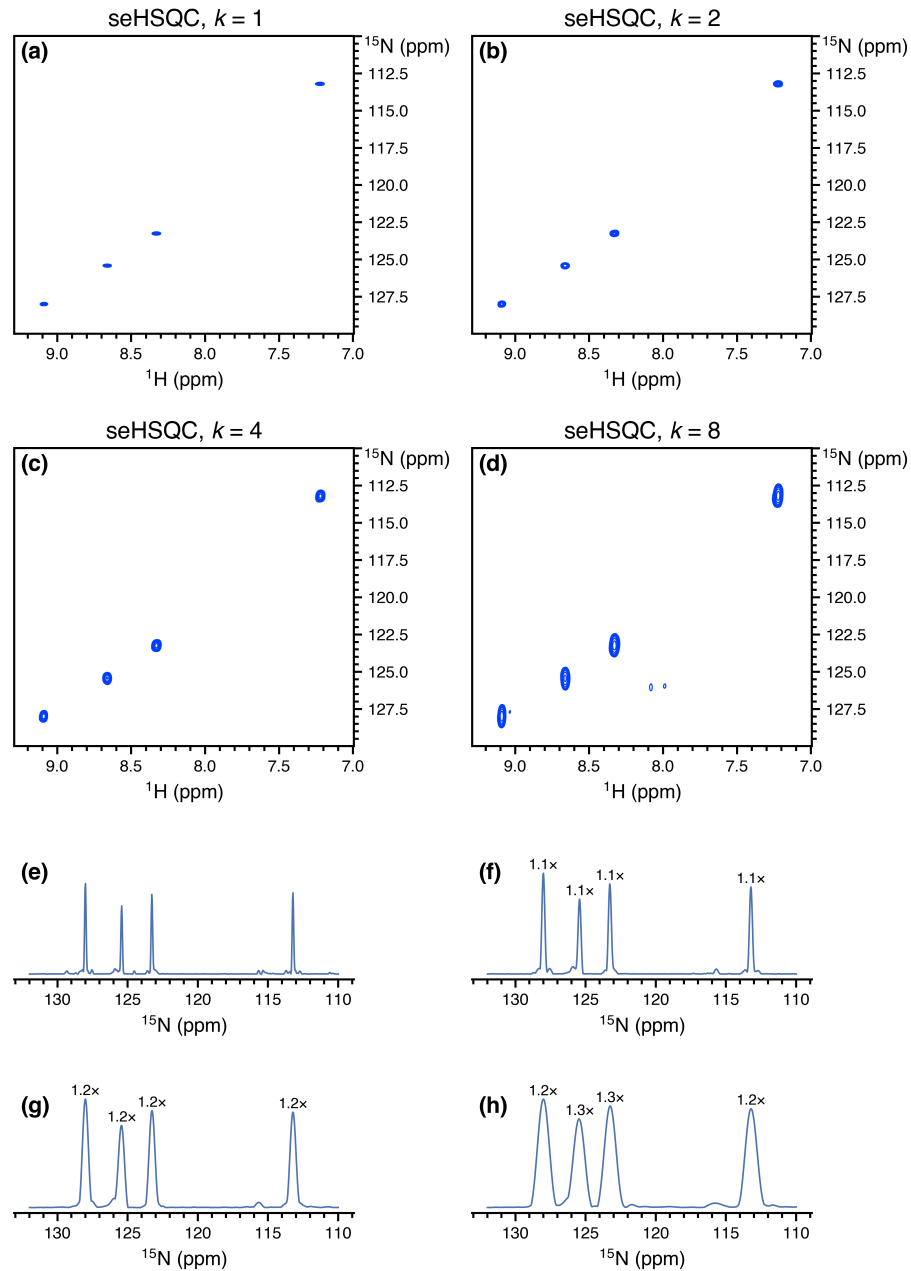


Figure S13: (seHSQC without linear prediction.) ^{15}N seHSQC spectra (from NOAH-3 $\text{S}_\text{N}^+\text{S}_2^+\text{C}^\text{c}$ super-sequences) obtained with various values of the scaling factor k . The peak at $\delta_\text{H} = 8.03$ ppm is a folded peak from the ornithine δ -NH₂. (a) $k = 1$ (256 t_1 increments, 2 scans each). (b) $k = 2$ (128 : 4). (c) $k = 4$ (64 : 8). (d) $k = 8$ (32 : 16). (e)–(h) Projections of 2D spectra in (a)–(d) onto the f_1 axis, shown at the same noise level. Numbers indicate peak heights relative to the $k = 1$ seHSQC spectrum. Spectra were obtained on a 700 MHz Bruker AV III equipped with a TCI H/C/N cryoprobe; the sample used was 40 mM gramicidin in DMSO-*d*₆.

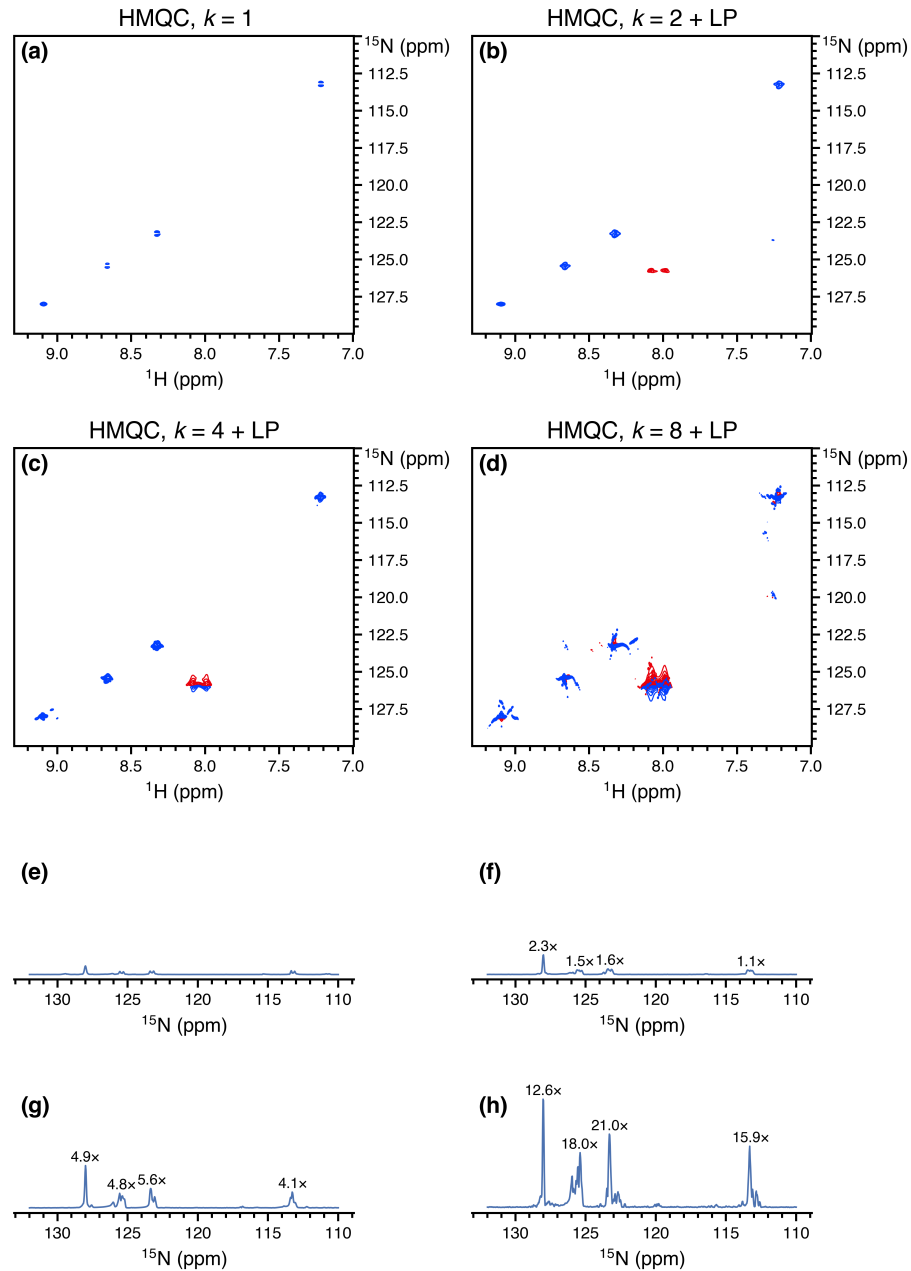


Figure S14: (HMQC with linear prediction.) ^{15}N HMQC spectra (from NOAH-3 $\text{MS}_2^+\text{C}^\text{c}$ supersequences) obtained with various values of the scaling factor k , after linear prediction up to 512 complex points in f_1 . The peak at $\delta_{\text{H}} = 8.03$ ppm is a folded peak from the ornithine $\delta\text{-NH}_2$. (a) $k = 1$ (256 : 2). Note that this spectrum is the same as in Figure S12a. (b) $k = 2$ (128 : 4). (c) $k = 4$ (64 : 8). (d) $k = 8$ (32 : 16). (e)–(h) Projections of 2D spectra in (a)–(d) onto the f_1 axis, shown at the same noise level. Numbers indicate peak heights relative to the $k = 1$ HMQC spectrum. Spectra were obtained on a 700 MHz Bruker AV III equipped with a TCI H/C/N cryoprobe; the sample used was 40 mM gramicidin in $\text{DMSO}-d_6$.

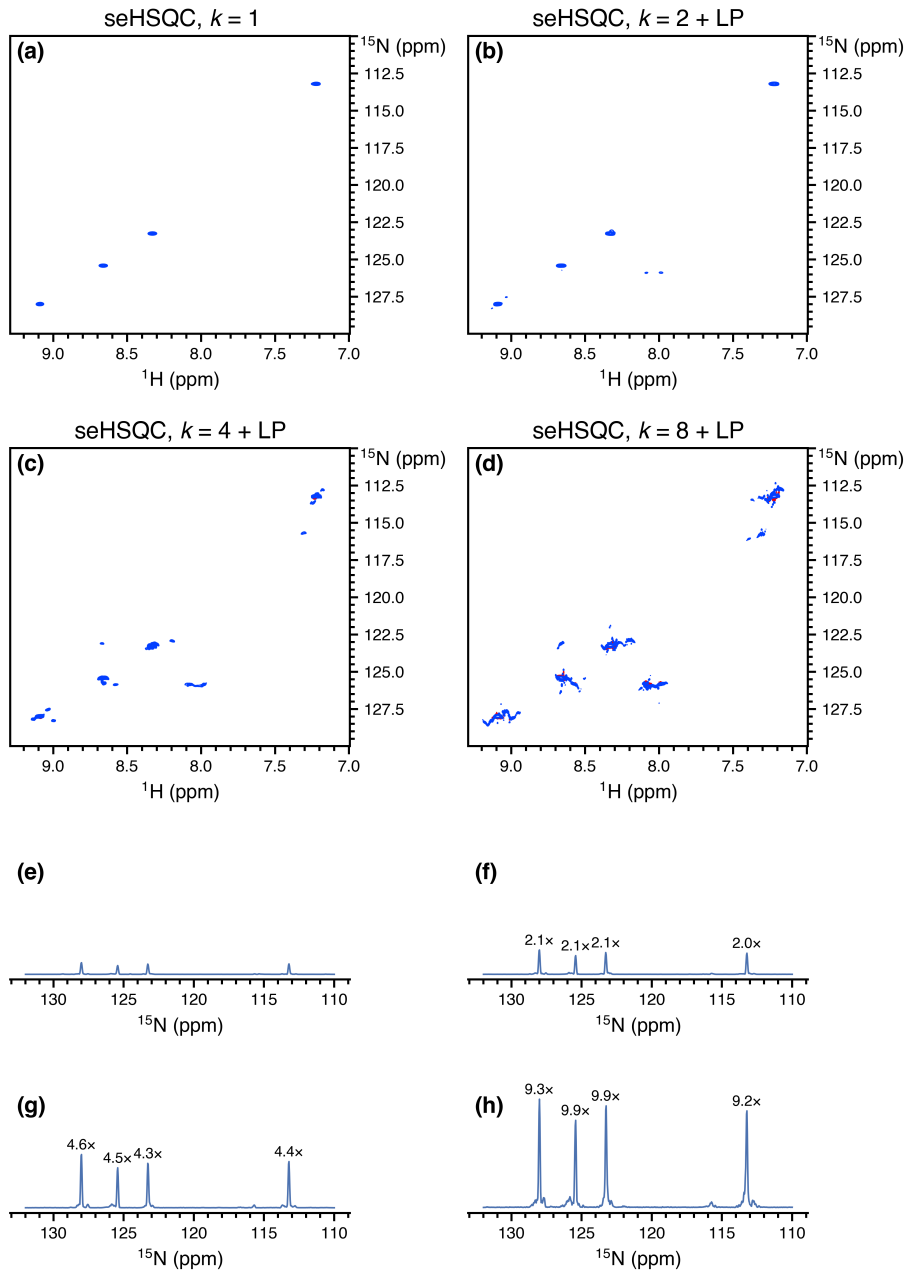


Figure S15: (seHSQC with linear prediction.) ^{15}N seHSQC spectra (from NOAH-3 $\text{S}_\text{N}^+\text{S}_2^+\text{C}^\text{c}$ supersequences) obtained with various values of the scaling factor k , after linear prediction up to 512 complex points in f_1 . The peak at $\delta_\text{H} = 8.03$ ppm is a folded peak from the ornithine $\delta\text{-NH}_2$. (a) $k = 1$ (256 : 2). Note that this spectrum is the same as in Figure S13a. (b) $k = 2$ (128 : 4). (c) $k = 4$ (64 : 8). (d) $k = 8$ (32 : 16). (e)–(h) Projections of 2D spectra in (a)–(d) onto the f_1 axis, shown at the same noise level. Numbers indicate peak heights relative to the $k = 1$ seHSQC spectrum. Spectra were obtained on a 700 MHz Bruker AV III equipped with a TCI H/C/N cryoprobe; the sample used was 40 mM gramicidin in $\text{DMSO}-d_6$.

11 HSQC-TOCSY/HSQC sensitivity comparisons

The signal intensities for the NOAH-3 S^TSC^c (HSQC-TOCSY + HSQC + CLIP-COSY) supersequences can be more conveniently measured by omitting the DIPSI-2 isotropic mixing in the HSQC-TOCSY supersequence, leading to a NOAH-3 SSC^c (HSQC + HSQC + CLIP-COSY) supersequence. This allows us to compare the different versions of double-HSQC sequences, as the two HSQC modules can be implemented either using the MFA approach, or the new ASAP/NOAH approach based on Ernst angle excitation in the first module. In the latter implementation, the parameter f can be varied between 0.4 and 1; it represents the proportion of $^1\text{H}^{\text{C}}$ magnetisation used in the first HSQC, as described in the main text. Furthermore, to boost the sensitivity of the second HSQC module in the NOAH supersequences, either of the two new seHSQC modules can be used in its place: we demonstrate this here with the ZIP-seHSQC (S_2^+).

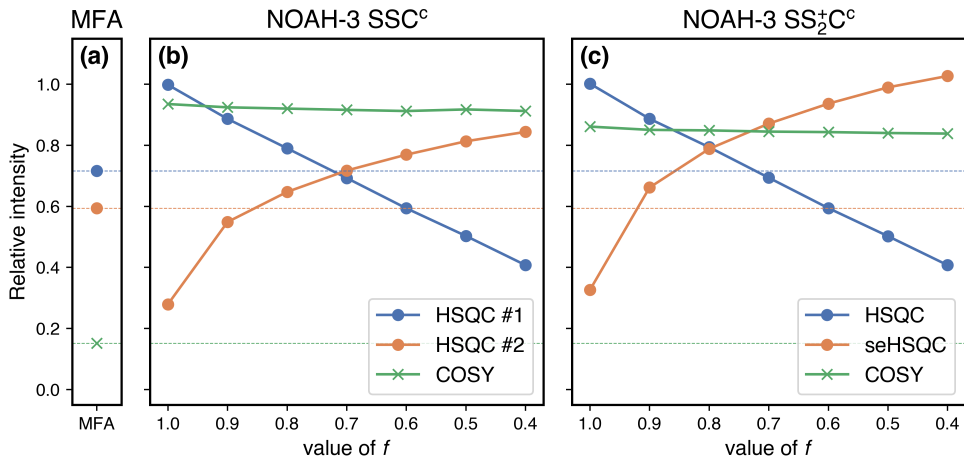


Figure S16: Sensitivities of HSQC and CLIP-COSY modules when used as part of a SSC^c-type supersequence, with both the NOAH and MFA implementations of the two HSQC modules. Intensities are calculated relative to the HSQC and CLIP-COSY modules in a standard NOAH-2 SCc supersequence (averaged over all peaks). (a) Sensitivity of the MFA implementation (i.e. a MFA double HSQC experiment immediately followed by a CLIP-COSY). Horizontal dashed lines at these levels are drawn across all subplots to guide the eye. (b) Sensitivity of NOAH-3 SSC^c modules as a function of f . Note that at $f = 0.8$, all of the NOAH spectra have a greater average sensitivity than their MFA counterparts. (c) Sensitivity of NOAH-3 SS₂⁺C^c modules as a function of f . Spectra were obtained on a 700 MHz Bruker AV III equipped with a TCI H/C/N cryoprobe; the sample used was 40 mM andrographolide in DMSO-*d*₆.

Figure S16 may be understood in the following way:

- The MFA HSQC sensitivities (in (a)) are approximately half that of a standard CRK seHSQC, with the second HSQC having slightly lower sensitivity. This is discussed in ref. 17 of the main text.
- The sensitivity of the first NOAH HSQC (blue in (b) and (c)) is generally equal to f , sup-

porting the interpretation of f as the fraction of $^{13}\text{C}-^1\text{H}$ magnetisation excited in the first HSQC.

- The sensitivity of the second NOAH HSQC (orange in (b)) arises from whatever is *not* used by the first HSQC, plus any magnetisation that relaxes during the FID of the first HSQC. As f is decreased, the former contribution increases and the latter tapers off. This is true for the seHSQC as well (orange in (c)), except that there is a uniform boost in sensitivity for all values of f . This sensitivity improvement mainly applies to CH groups, as discussed in the main text.
- The MFA COSY sensitivity (green) is substantially lower ($\sim 15\%$) because the bulk magnetisation is dephased by the previous modules, whereas in the NOAH approach it is (largely) preserved.

It remains to evaluate the impact of adding DIPSI-2 mixing in one of the HSQC modules on the remaining modules in the supersequence. This depends on whether the HSQC-TOCSY module is placed first ($S^T\text{SC}^c$ or $S^T\text{S}_2^+C^c$) or second ($SS^T\text{C}^c$) in the sequence. Since neither of the new seHSQC modules do preserve unused $^1\text{H}^C$ magnetisation, the HSQC-TOCSY in a hypothetical $S^+S^T\text{C}^c$ supersequence will have greatly reduced sensitivity. On the other hand, placing the HSQC-TOCSY sequence first allows the seHSQC module to be used subsequent to this; we therefore consider only the permutations where the HSQC-TOCSY goes first.

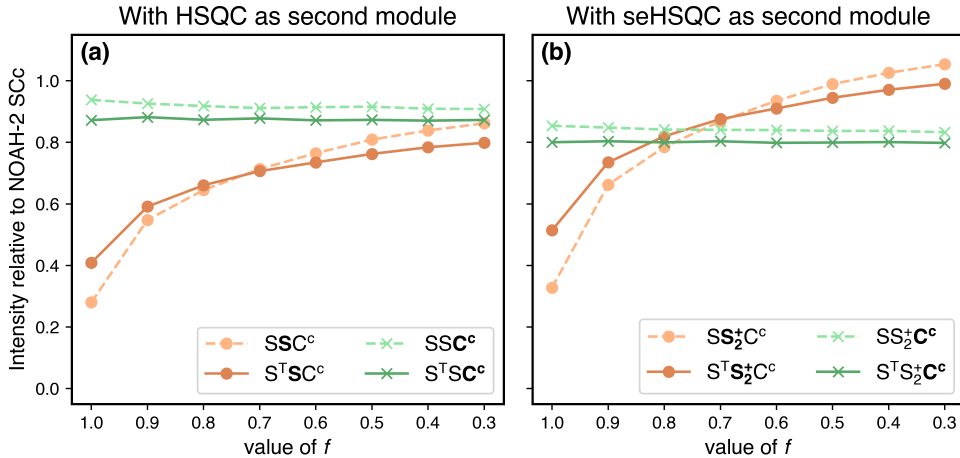


Figure S17: Comparison of signal intensities of second (HSQC or seHSQC) and third (CLIP-COSY) modules in the $S^T\text{SC}^c$ and $S^T\text{S}_2^+C^c$ supersequences, versus their intensities in the SSC^c and $\text{SS}_2^+C^c$ sequences, as a function of the parameter f . The solid, darker lines indicate the supersequences beginning with the HSQC-TOCSY, whereas the dashed, lighter lines indicate the supersequences beginning with the HSQC (the latter are the same graphs as in Figure S16). **(a)** With the HSQC as the second module. **(b)** With the seHSQC as the second module. Spectra were obtained on a 700 MHz Bruker AV III equipped with a TCI H/C/N cryoprobe; the sample used was 40 mM andrographolide in $\text{DMSO}-d_6$.

It can be seen from Figure S17 that the introduction of DIPSI-2 mixing leads to a very small drop (< 10%) in the amount of $^1\text{H}^{1\text{C}}$ magnetisation preserved for the COSY module. On the other hand, the HSQC (and seHSQC) sensitivities follow largely the same trend as before. For values of f above 0.7 (where relatively little $^1\text{H}^{1\text{C}}$ magnetisation is preserved for these modules), the DIPSI-2 mixing helps to replenish some of this magnetisation. As f decreases, this effect becomes smaller, and at small f it even leads to a reduction in signal intensity. As discussed in the main text, since the HSQC-TOCSY has a lower intrinsic sensitivity than the (se)HSQC, we recommend using a large value of f , such as 0.9. This does not compromise the HSQC-TOCSY intensity by much, and at the same time yields either a HSQC with $\sim 60\%$ of its original sensitivity, or a seHSQC which has $\sim 75\%$ of the sensitivity of a standard NOAH HSQC.

If the sensitivity of the HSQC-TOCSY component is to be maximised, then it is advisable to use the seHSQC-TOCSY module, which is based on the S_2^+ module and is described in ref. 14 of the main text. This module cannot preserve any $^1\text{H}^{1\text{C}}$ magnetisation for the downstream HSQC, but does retain $^1\text{H}^{1\text{C}}$ magnetisation for homonuclear modules: its performance in this respect is therefore very similar to the HSQC-TOCSY with $f = 1$ (Figure S18). However, it provides greater sensitivity in the HSQC-TOCSY component itself, so is strictly better than the HSQC-TOCSY with $f = 1$.

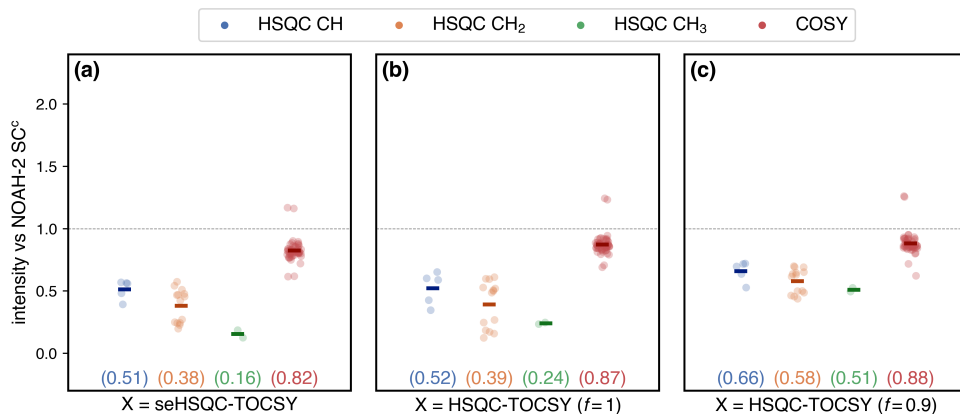


Figure S18: HSQC and COSY intensities in NOAH-3 XSC^c supersequences, where X is a HSQC-TOCSY variant, normalised against the intensities of the NOAH-2 SC^c. (a) With X as the seHSQC-TOCSY module, derived from the S_2^+ sequence. (b) With the unenhanced HSQC-TOCSY module ($f = 1$). Note that this provides no improvement over the seHSQC-TOCSY in the downstream HSQC and COSY modules. (c) With the unenhanced HSQC-TOCSY module ($f = 0.9$). This retains a portion of unused $^1\text{H}^{1\text{C}}$ magnetisation for the second HSQC, resulting in higher intensities. Spectra were obtained on a 700 MHz Bruker AV III equipped with a TCI H/C/N cryoprobe; the sample used was 40 mM andrographolide in DMSO-*d*₆.

Finally, we note that because a significant proportion of the HSQC signal derives from $^1\text{H}^{1\text{C}}$ relaxation during the HSQC-TOCSY FID, use of a longer acquisition time (AQ) can potentially boost the HSQC sensitivity even further. The experiments shown above were carried out with a relatively short AQ of 73 ms. **However, bear in mind that the high duty cycle associated**

with broadband ^{13}C decoupling can potentially damage the probe if applied for too long, especially given that the supersequences described here have two consecutive ^{13}C -decoupled modules.

12 Other example spectra

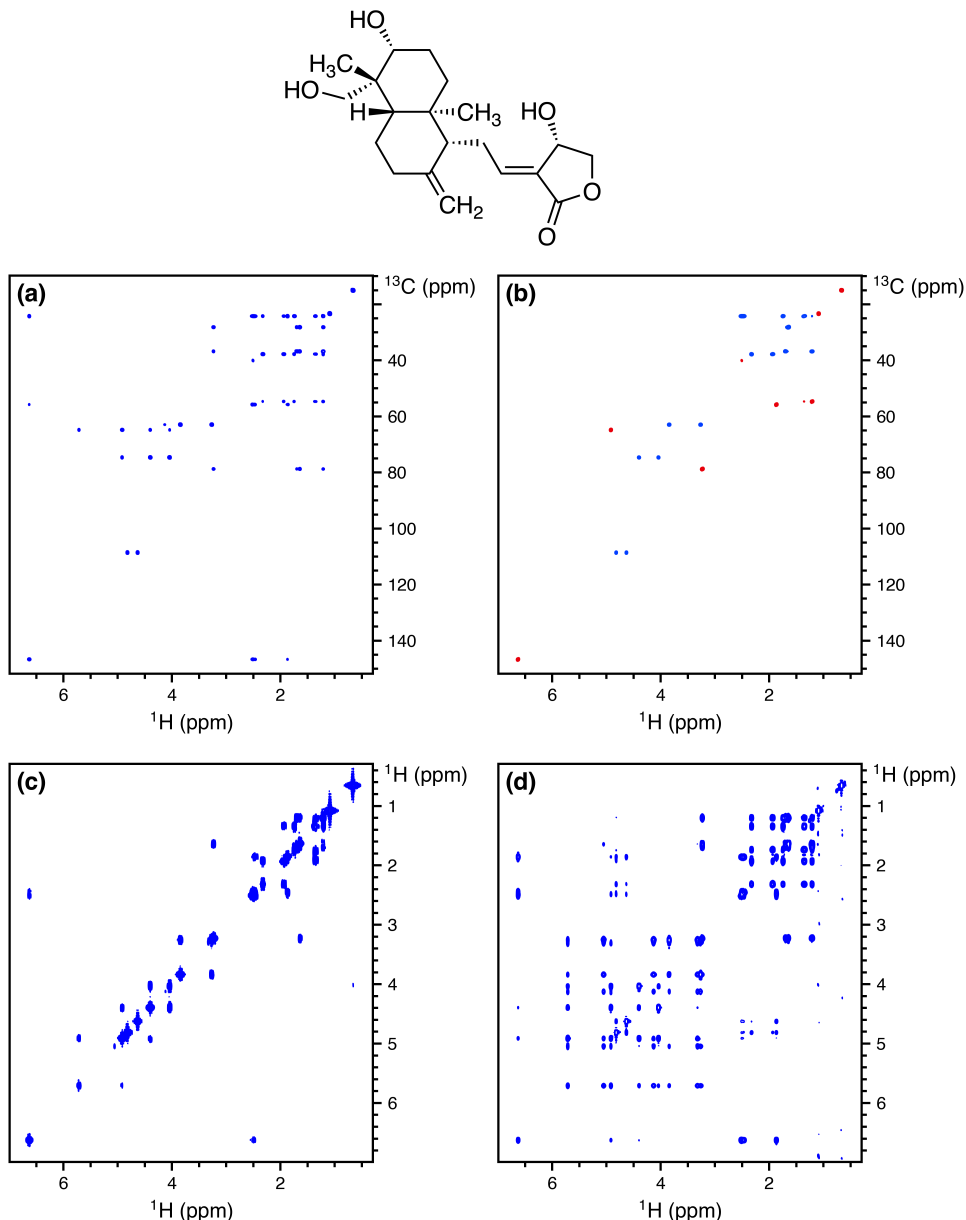


Figure S19: 2D spectra acquired using the NOAH-4 $S^T S_2^+ CT$ supersequence. 256 t_1 increments were used with 2 scans per increment, leading to a total experiment time of 17 minutes and 32 seconds. This represents a 3.25 \times time saving relative to conventional acquisition of each of the four spectra with the same parameters, which would take a total of 57 minutes and 3 seconds. (a) HSQC-TOCSY (30 ms mixing time, $f = 0.9$). (b) Multiplicity edited seHSQC. (c) COSY. (d) TOCSY (60 ms mixing time). Spectra were obtained on a 700 MHz Bruker AV III equipped with a TCI H/C/N cryoprobe; the sample used was 40 mM andrographolide in DMSO- d_6 .

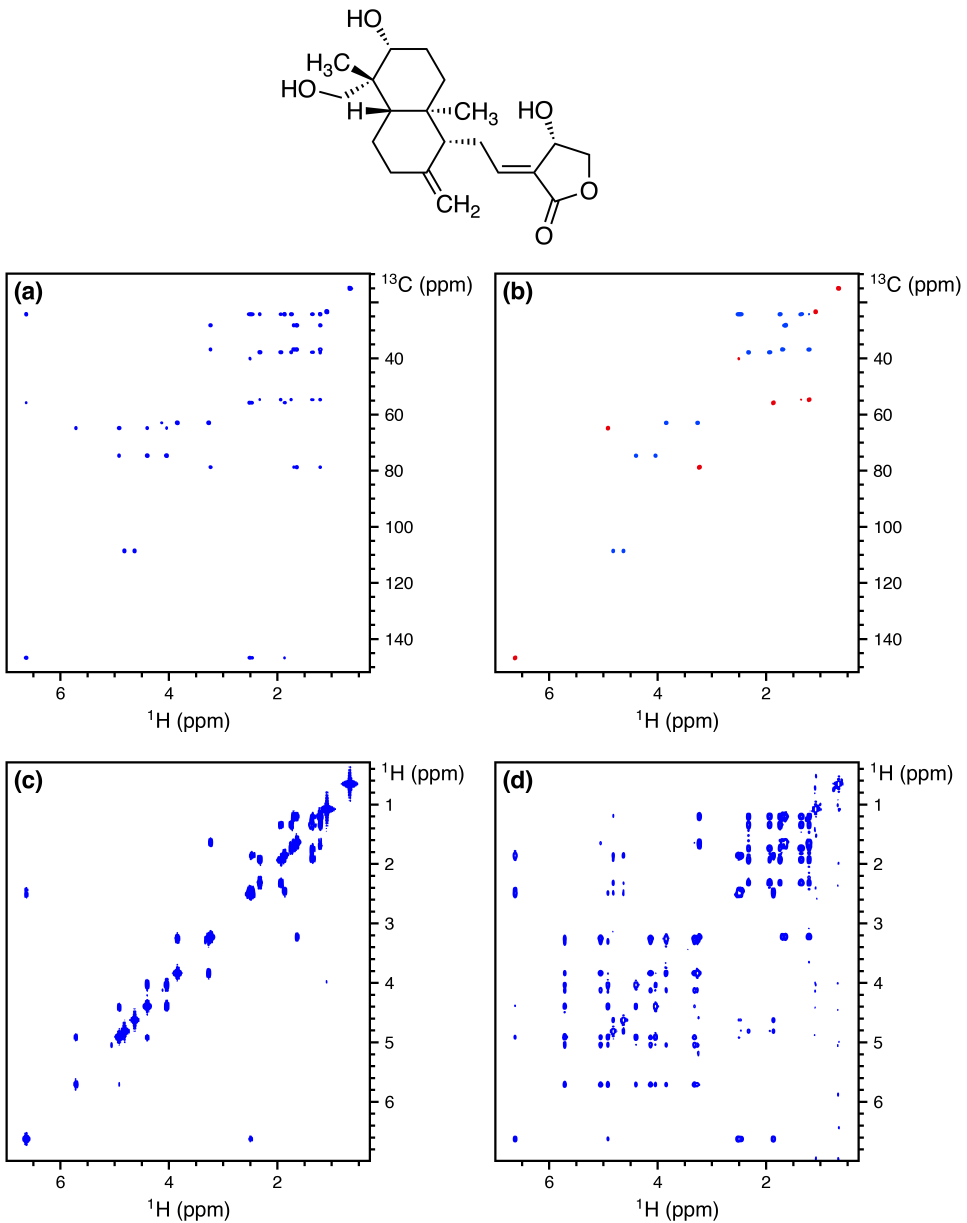


Figure S20: 2D spectra acquired using the NOAH-4 S^TS₂⁺CT supersequence with 50% non-uniform sampling for all modules. All other parameters are the same as in Figure S19. The experimental time was 9 minutes and 1 second. (a) HSQC-TOCSY (30 ms mixing time, $f = 0.9$). (b) Multiplicity edited seHSQC. (c) COSY. (d) TOCSY (60 ms mixing time). Spectra were obtained on a 700 MHz Bruker AV III equipped with a TCI H/C/N cryoprobe; the sample used was 40 mM andrographolide in DMSO-*d*₆.

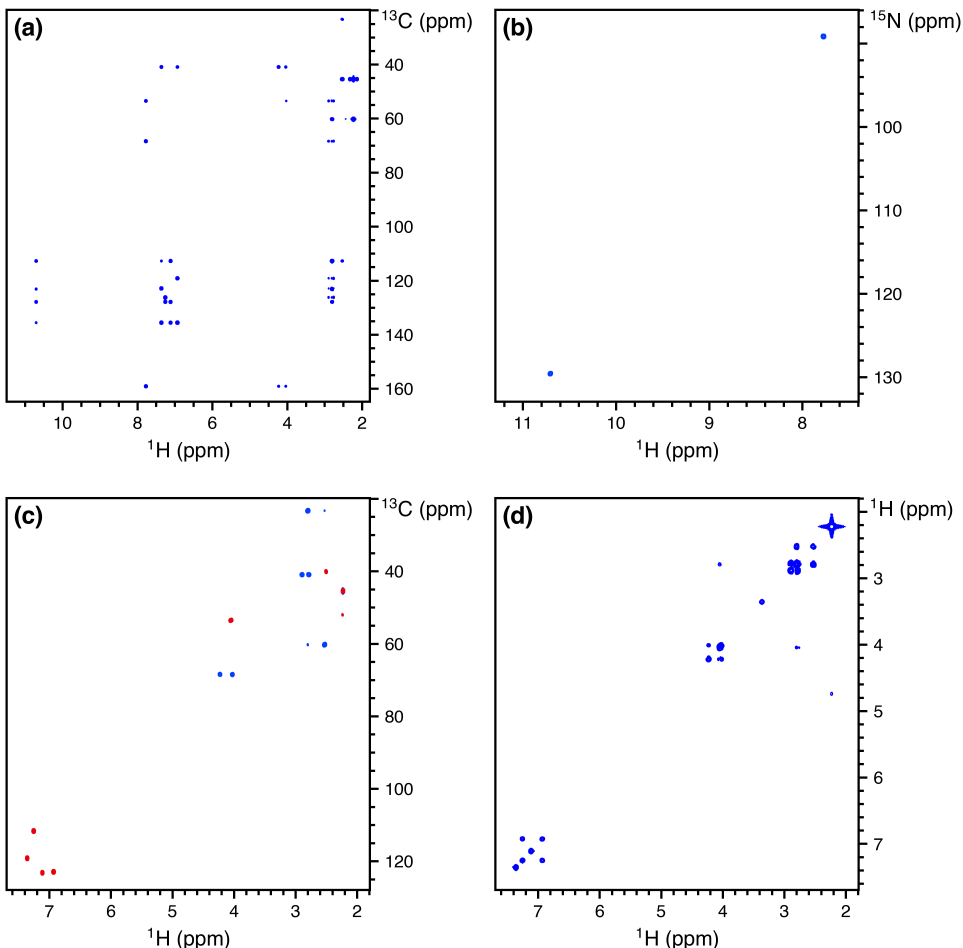
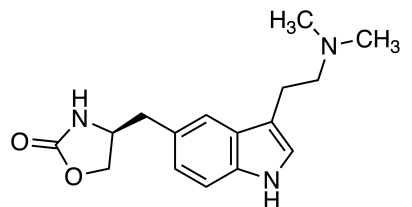


Figure S21: 2D spectra acquired using the NOAH-4 BS_{N2}⁺S₂⁺C supersequence. 256 t_1 increments were used with 2 scans per increment, leading to a total experiment time of 17 minutes and 32 seconds. This represents a 3.22× time saving relative to conventional acquisition of each of the four spectra with the same parameters, which would take a total of 56 minutes and 28 seconds. (a) HMBC. (b) ¹⁵N seHSQC with $k = 4$, linear projected to 512 complex points. (c) Multiplicity edited ¹³C seHSQC. (d) Magnitude-mode COSY (Bruker qf mode). Spectra were obtained on a 700 MHz Bruker AV III equipped with a TCI H/C/N cryoprobe; the sample used was 50 mM zolmitriptan in DMSO-*d*₆.